2021 60th IEEE Conference on Decision and Control (CDC)
December 13-15, 2021. Austin, Texas

Collision Avoidance and Rendezvous of Quadric Surfaces Moving on Planar Environments

Kashish Dhal[1] Abhishek Kashyap[1] Animesh Chakravarthy[1]

2021 60th IEEE Conference on Decision and Control (CDC) | 978-1-6654-3659-5/21/$31.00 ©2021 IEEE | DOI: 10.1109/CDC45484.2021.9683549

Abstract— **Achieving collision avoidance or rendezvous between moving objects are important objectives in robotic systems. In performing collision avoidance or rendezvous maneuvers, the relative shapes of the objects play an important role. The literature largely models the shapes of the objects as circles, and this can make the maneuvers very conservative, especially when the objects are of elongated shape. In this paper, we model the shapes of the objects using quadric surfaces. A collision/rendezvous cone concept is employed. A computationally efficient approach to compute the collision/rendezvous cone between finite-sized quadric surfaces (which are not necessarily of the same shape) is presented. Nonlinear analytical guidance laws that perform collision avoidance or rendezvous maneuvers, are subsequently developed. Simulation results demonstrating the working of the developed guidance laws are presented.**

I. INTRODUCTION

An important component of robot path planning is the collision avoidance problem, that is, determining a safe trajectory of a robotic vehicle so that it circumvents various stationary and dynamic obstacles in its path. When the robot and obstacles are operating in close proximity, their relative shapes can play an important role in the determination of collision avoidance trajectories. One common practice is to use polygonal approximations as bounding boxes for the shapes of the robots and obstacles. However, the polygonal approximation can lead to increased computational complexity (measured in terms of obstacle complexity, or the amount of information used to store a computer model of the obstacle, where obstacle complexity is measured in terms of the number of obstacle edges [1]). To overcome this, a common practice then is to use circular approximations for the robots and the obstacles, because of the analytical convenience such approximations provide, along with the reduced information required to store a computational model of the obstacle. The obstacle avoidance conditions are then computed for the circle as a whole.

These approximations become overly conservative in cases when an object is more elongated along one dimension compared to another. In such cases, non-circular objects such as ellipses have been used to serve as better approximations for the object shapes [2], [3], [4], [5]. For non-convex objects however, even elliptical approximations can become over conservative, because such approximations reduce the amount of available free space within which the robot trajectories can lie in which case, one can take recourse to non-convex bounding approximations involving a combination of an ellipse and a hyperbola.

This paper employs a collision cone based approach to determine analytical expressions of collision avoidance laws for moving objects whose shapes are modeled by quadric surfaces. The collision cone approach, originally introduced in [6], has some similarities with the velocity obstacle approach [7] in that both approaches determine the set of velocities of the robots that will place them on a collision course with one or more obstacles. However while the velocity obstacle approach, and its many extensions [8], has been restricted to circles/spheres, the fact that the collision cone approach has its roots in missile guidance, enables it to determine closed form collision conditions for a large class of object shapes. In [6], conditions that are both necessary and sufficient for collision of two arbitrarily shaped objects moving on a plane were determined, while in [9],[10] conditions that are necessary and sufficient for collision of a point object with a quadric surface moving in 3-D space were determined. The great benefit of obtaining analytical expressions of collision conditions is that these then serve as a basis for determining analytical expressions of collision avoidance laws. Such analytical expressions can lead to tremendous computational savings, especially in multi-obstacle environments.

When both agents are quadric surfaces of different shapes, one can perform a Minkowski sum operation to superpose the shape of one object onto the other, thereby reducing the first object to a point, while growing the second object. However, the Minkowski sum operation can be computationally expensive. In contrast, the current paper develops an analytical approach to compute the collision cone between quadric surfaces moving on a plane, without taking recourse to computing the Minkowski sum. Acceleration laws for collision avoidance and rendezvous of quadric surfaces are subsequently developed.

The collision cone approach of [6] has been extensively employed in the literature, for example, in driver assistance systems [11], safe trajectories for aircraft [12], tracking a moving target [13], multi-vehicle collision avoidance problem [14], investigation of collision avoidance and guidance in biological systems such as fish [15]-[16].

The rest of this paper is organized as follows. Section II provides a review of the collision avoidance results for arbitrary objects moving on a plane, as determined in [6]. The contribution of this paper begins from Section III, which shows the computation of the collision cone when

This work was supported by a grant from the National Science Foundation IIS-1851817.

[1]Kashish Dhal, Abhishek Kashyap and Animesh Chakravarthy are with the Department of Mechanical and Aerospace Engineering, University of Texas at Arlington, TX, USA kashish.dhal@mavs.uta.edu, abhishek.kashyap@mavs.uta.edu, animesh.chakravarthy@uta.edu

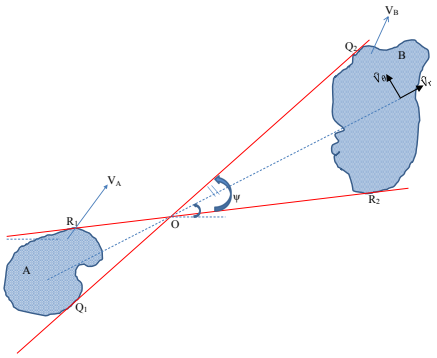

Fig. 1. Engagement geometry between arbitrarily shaped objects

the objects are modeled by quadric surfaces. Section V presents simulations that demonstrate the working of these acceleration laws, while Section VI presents the conclusions.

II. Background on the Collision Cone

Refer Fig 1, which shows two arbitrarily shaped objects A and B moving with velocities V_A and V_B, respectively. The lines Q_1Q_2 and R_1R_2 form a sector with the property that this represents the smallest sector that completely contains A and B such that A and B lie on opposite sides of the point of intersection O. Let $\hat{V}_r$ and $\hat{V}_\theta$ represent the relative velocity components of the angular bisector of this sector, as shown. As demonstrated in [6], A and B are on a collision course if their relative velocities belong to a specific set. This set is encapsulated in a quantity y defined as follows:

$$y = \frac{\hat{V}_\theta^2}{(\hat{V}_\theta^2 + \hat{V}_r^2)} - \sin^2\left(\frac{\psi}{2}\right) \tag{1}$$

The collision cone is defined as the region in the $(\hat{V}_\theta, \hat{V}_r)$ space for which $y < 0$, $\hat{V}_r < 0$ is satisfied. Thus, any relative velocity vector satisfying this condition lies inside the collision cone. The condition corresponding to $y = 0$, $\hat{V}_r < 0$ defines the boundaries of the collision cone and any relative velocity vector satisfying this condition is aligned with the boundary of the collision cone.

III. Computing the Collision and Rendezvous Cones between Quadric Surfaces

A challenge in computing the collision cone for arbitrarily shaped objects is in the computation of the sector enclosing the objects A and B (shown in Fig 1), and determination of the angle ψ. Note that as A and B move, the angle ψ changes with time. An iterative method to determine ψ for arbitrarily shaped objects using the concept of conical hulls was presented in [17]. In this paper, we present an approach to compute ψ for objects that can be modeled by quadric surfaces. This approach is computationally inexpensive which makes it very suitable for real-time implementation.

A. Collision cone between two ellipses

An ellipse is represented by a general equation of the form:

$$ax^2 + bxy + cy^2 + dx + ey + f = 0 \tag{2}$$

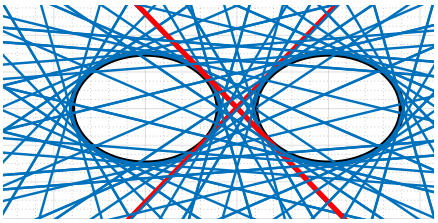

Fig. 2. Dual Space

The above can be written in matrix form as follows:

$$\begin{bmatrix} x & y & 1 \end{bmatrix} \begin{bmatrix} a & b/2 & d/2 \\ b/2 & c & e/2 \\ d/2 & e/2 & f \end{bmatrix} \begin{bmatrix} x \\ y \\ 1 \end{bmatrix} = 0 \tag{3}$$

which can be written compactly as: $\mathbf{x}^T M\mathbf{x} = 0$. For any given point $\mathbf{p}$ on the ellipse, $\mathbf{l} = M\mathbf{p}$ represents the homogeneous coordinates of the tangent to the ellipse at that point. The equation of the tangent line is then obtained as $\mathbf{l}^T\mathbf{x} = 0$. The dual of the ellipse $\mathbf{x}^T M\mathbf{x} = 0$ is defined as the set of tangents to the given ellipse, and is obtained as follows [18]:

$$\begin{aligned} &\mathbf{p}^T M\mathbf{p} = 0 \,(\text{Definition of ellipse}) \\ \Rightarrow\ &\mathbf{p}^T MM^{-1}M\mathbf{p} = 0 \Rightarrow \mathbf{l}^T M^{-1}\mathbf{l} = 0 \end{aligned} \tag{4}$$

Thus, any line satisfying (4) belongs to the tangent set of the ellipse, described by M.

Now, consider the scenario involving two ellipses, whose equations are $\mathbf{x}^T M_1\mathbf{x} = 0$ and $\mathbf{x}^T M_2\mathbf{x} = 0$. To find the common tangents to these two ellipses, we need to find the lines $\mathbf{l}$ which simultaneously satisfy the two equations, $\mathbf{l}^T M_1^{-1}\mathbf{l} = 0$, and $\mathbf{l}^T M_2^{-1}\mathbf{l} = 0$. See Fig 2. This leads to two coupled quadratic equations which have to be solved for the unknown $\mathbf{l}$. While this presents a viable method to compute the common tangents to the two ellipses (and hence the angle ψ), it is still computationally expensive to solve for real-time operations. However, by employing the concept of degenerate conics (discussed subsequently), a solution can be found using elementary linear algebraic operations and this reduces the computation time.

Finding the homogeneous coordinates of the common tangents to the two ellipses requires finding the intersections between their corresponding duals. Toward this end, defining $C_1 = M_1^{-1}$ and $C_2 = M_2^{-1}$, the pencil of dual conics is formed from $C_1 - tC_2$, where t is a real number. This pencil represents the family of all dual conics which pass through their intersection points.

A degenerate conic is formed by two lines that may or may not be parallel. The degenerate conics obtained from the above pencil, occur at those values of t for which $det(C_1 - tC_2) = 0$. Since this is a polynomial equation of degree 3 in t, there are therefore three possible solutions. The above pencil thus has three degenerate conics, and these correspond to three pairs of lines.

The intersection point, $\mathbf{u}$, of each pair of lines is obtained as a solution to the equation $(C_1 - tC_2)\mathbf{u} = 0$. By multiplication of C_2^{-1} on both sides, this equation becomes $(C_2^{-1}C_1 - t\ I)\mathbf{u} = 0$, which implies that t is an eigenvalue of $C_2^{-1}C_1$ and $\mathbf{u}$ is the corresponding eigenvector. We note that

calculating the eigenvalues of the matrix $C_2^{-1}C_1$ and their corresponding eigenvectors is computationally inexpensive, when compared to using a numeric solver to solve $\mathbf{l}^T M_1^{-1}\mathbf{l} = 0$, and $\mathbf{l}^T M_2^{-1}\mathbf{l} = 0$.

We concatenate the 3 eigenvectors to form a 3×3 matrix U. Next, conjugating $C_1 - tC_2$ by U will perform a projective transformation that sends the first two intersection points of the degenerate conics (contained in the first two columns of U) to infinity and the third intersection point (contained in the third column of U) to the origin. The special coordinate system formed after this projective transformation converts the three pairs of lines into a rectangle. The sides of this rectangle are formed by the first two columns of U (first two degenerate conics) and the diagonals of this rectangle are formed by the third column of U (third degenerate conic).

The homogeneous coordinates of the common tangent lines are now represented by the vertices of this rectangle. We hence get four tangent lines from this rectangle. These four tangent lines are then projected back to the homogeneous coordinate system.

The next step is to find the two inner common tangent lines. We know that the inner common tangents will have the centers of the two ellipses on opposite sides of the tangent line, while the outer common tangents will have the the centers of both ellipses on the same side of the tangent line. We use this fact to extract the inner common tangents out of the four solutions obtained. Once we get the homogeneous equations of the inner common tangents, we can find the angle between them.

B. Collision cone between an ellipse and a confocal quadric

1) Confocal quadric description: A confocal quadric surface is formed by a pair of quadric surfaces which share the same focal points. One such confocal quadric, formed by the intersection of an ellipse and a hyperbola (both sharing the same foci) is schematically represented in Fig 3 (a). It is a non-convex object and is represented by the equation:

$$\begin{aligned} &\left(\frac{x'}{a_c}\right)^2 + \left|\left(\frac{y'}{b_c}\right)^2 - k\right| = 1, k \in [0,1] \\ \text{where} \quad & x' = (x-x_1)\cos(\phi) + (y-y_1)\sin(\phi) \\ \text{and} \quad & y' = -(x-x_1)\sin(\phi) + (y-y_1)\cos(\phi) \end{aligned} \tag{5}$$

Here, x_1 and y_1 are the coordinates of the center of the confocal quadric and ϕ is the angle which the line joining it's foci makes with respect to the x axis in the cartesian plane. The lengths of the semi-major and semi-minor axes of the ellipse are given by $a_c\sqrt{1+k}$ and $b_c\sqrt{1+k}$, respectively. The lengths of the semi-major and semi-minor axes of the hyperbola are given by $a_c\sqrt{1-k}$ and $b_c\sqrt{1-k}$, respectively.

By varying the parameter k between 0 and 1, the object exhibits a continuous shape and size transformation. These are shown in Fig 3 (b). The two extreme values of k correspond to two special cases. When $k = 0$, then (5) represents an ellipse whose semi-major and semi-minor axes have lengths a_c and b_c respectively. When $k = 1$, the hyperbola degenerates into a pair of intersecting lines and the resulting shape is as shown in Fig. 3 (b). The four corner points of the confocal quadric are marked as A, B, C and D in Fig 3 (a).

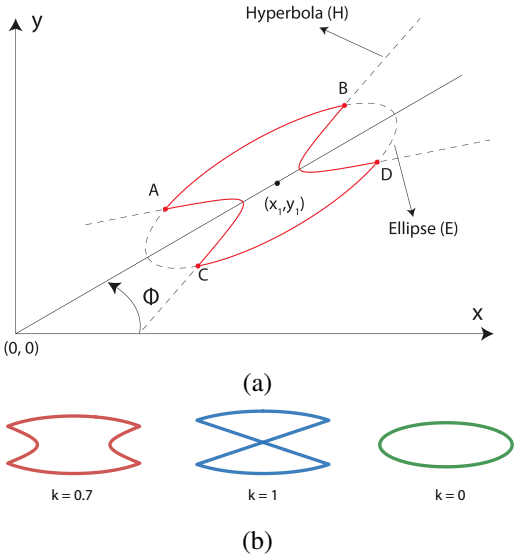

Fig. 3. (a) Confocal Quadric, (b) Confocal Quadric with Varying k

2) Common tangents computation: This section describes computation of the inner common tangents between an ellipse F_1 and a confocal quadric F_2'. Let F_2 represent the ellipse which is associated with F_2'.

In the first step, common tangents are computed between F_1 and F_2 using the algorithm given in the previous subsection. Two different cases then arise. In the first case, both common tangents lie on F_2'. In this case, the resulting tangents can be accepted as a valid solution.

In the second case, one or both common tangents lie on F_2, but not on F_2'. In this case, the corresponding common tangent(s) should pass through one of the four corner points. (This is because the tangents cannot lie on the hyperbolic portion of F_2', since that portion is concave.) Find a new tangent to F_1 passing through each corner point using the concept of polar and poles. Let (u,v) represent the cartesian coordinates of the corner point from which we want to draw the tangents to F_1. Then, the homogeneous coordinates of this point are $\mathbf{p} = [u\ v\ 1]^T$. We can write $C_1 = F_1^{-1}$ and let $a' = F^{-1}(1,1)$, $b' = F^{-1}(2,2)$, $c' = F^{-1}(1,2)$, $d' = F^{-1}(1,3)$, $e' = F^{-1}(2,3)$, and $f' = F^{-1}(3,3)$. The pencil of lines through the corner point $\mathbf{p}$ can be parametrically written in terms of γ as $\mathbf{t}(\gamma) = [-\sin(\gamma)\ \cos(\gamma)\ u\sin(\gamma) - v\cos(\gamma)]^T$. If $\mathbf{t}$ is a tangent to F_1 (meaning it belongs to the dual set of F_1), then it should satisfy $\mathbf{t}^T\ C_1\ \mathbf{t} = 0$. We can solve this equation to find two values of γ as follows:

$$\gamma = \frac{1}{2}\left(\tan^{-1}\left(\frac{K_1}{K_2}\right) \pm \left(\sin^{-1}\left(\frac{2K_0 + K_2}{\sqrt{K_1^2 + K_2^2}}\right) + \frac{\pi}{2}\right)\right)$$

$$\text{where } K_2 = (b'-a') + 2(d'u - e'v) + f'\left(v^2 - u^2\right)$$

$$K_0 = a'^2 - 2d'u + f'u^2,\ K_1 = -2\left(c' - (d'v' + e'u) + f'uv\right)$$

Also, the point of intersection of this tangent with F_1 is computed from the concept of polar as $\mathbf{q} = C_1\mathbf{t}$. Substituting

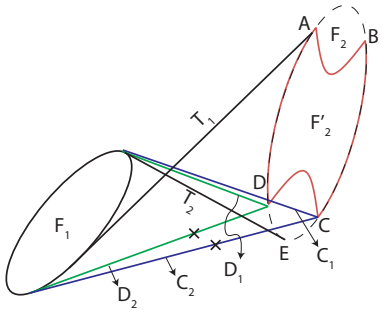

Fig. 4. Algorithm to choose correct tangent

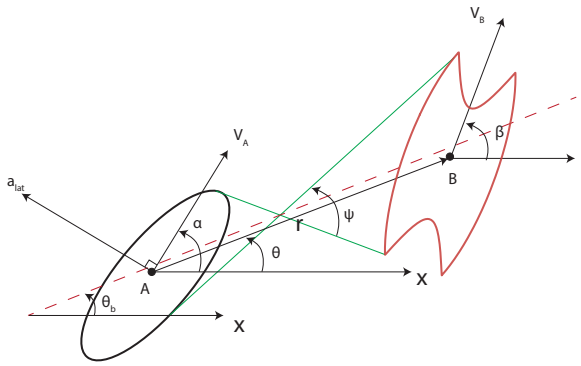

Fig. 5. Engagement Geometry between an ellipse and a confocal quadric

the value of γ in this equation we can find a solution for $\mathbf{q}$ as follows:

$$\mathbf{q} = \begin{pmatrix} (c' - d'v)\cos\gamma + (d'u - a')\sin\gamma \\ (b' - e'v)\cos\gamma + (e'u - c')\sin\gamma \\ (e' - f'v)\cos\gamma + (f'u - d')\sin\gamma \end{pmatrix} \tag{6}$$

The above represents an analytical equation which can be used to compute the two tangents to F_1 from a given corner point. (Note that this analytical equation obviates the need for computationally expensive solvers). Since there are four corner points, this means that in all there can be eight tangents to F_1 (two from each corner point). The question now is which of the eight tangents should be chosen for the computation of ψ. This will be explained with reference to Fig 4.

In the case depicted in Fig 4, tangent T_1 lies on F_2', while tangent T_2 lies on F_2, but not on F_2'. In this case, T_2 is therefore not a valid tangent (for the computation of ψ) and we therefore need to replace this with a tangent which originates from one of the corner points. For this we use the following algorithm:

1) First, determine if F_1 and F_2 intersect with each other
2)(a) If they do not intersect, search for the two corner points nearest to the original tangent point E. In Fig 4, these corner points are C and D.
   (b) If they do intersect, search for the two corner points nearest to the mid-point of the line joining the centers of F_1 and F_2.
3) From each of the two chosen corner points (C and D in Fig 4), draw two tangents to F_1. In Fig 4, these tangents are shown C_1, C_2, D_1 and D_2.
4) Out of the two tangents from each corner point, retain those tangent lines which create a separating hyper-plane such that centers of F_1 and F_2 lie on opposite sides of this hyper-plane. In Fig 4, we reject C_2 and D_2, marked by x because the centers of both F_1 and F_2 lie in the same half-space for each line. In the special case when F_1 and F_2' are grazing each other, both tangents from a single corner point may satisfy this property, and in such a case we keep both of them as the desired inner common tangent lines and skip step 5.
5) Then out of the remaining two tangents (C_1 and D_1 in Fig 4), we reject C_1 because it passes through F_2' (indicated by D and center of F_2' lying in opposite half-spaces of C_1), however D_1 does not pass through F_2' (indicated by C and center of F_2' lying in the same half-space of D_1).

Thus, we are left with two tangent lines D_1 and T_1, and these are the desired inner common tangents. In the scenario where the other tangent line T_1 also does not lie on F_2', we repeat the same algorithm to replace T_1 with a tangent from one of the corner points.

IV. Computation of Acceleration Laws to Achieve Collision Avoidance or Rendezvous

In this section, we derive analytical expressions for the acceleration laws required for collision avoidance or rendezvous (as the objective may be). Consider the engagement geometry shown in Fig 5. The objects A and B are an ellipse and a confocal quadric, moving with speeds V_A and V_B, respectively, and heading angles α and β, respectively. (We note that B could also be an ellipse, in which case the geometry would be one of engagement between two ellipses). The distance between the centers of A and B is represented by r, and the angle made by the line joining these centers is represented by θ. The control input of A is its lateral acceleration a_{lat}, which acts normal to the velocity vector of A. The kinematics governing the engagement geometry are characterized by the following equations:

$$\begin{bmatrix} \dot{r} \\ \dot{\theta} \\ \dot{V}_\theta \\ \dot{V}_r \\ \dot{\alpha} \end{bmatrix} = \begin{bmatrix} V_r \\ V_\theta / r \\ -V_\theta V_r / r \\ V_\theta^2 / r \\ 0 \end{bmatrix} + \begin{bmatrix} 0 \\ 0 \\ -\cos(\alpha - \theta) \\ \sin(\alpha - \theta) \\ 1/V_A \end{bmatrix} a_{lat,A} \tag{7}$$

Now we will use the kinematics of engagement geometry to define the collision cone. The inner common tangents are shown in green color in Fig 5 and the angle between these tangents is represented by ψ. The quantity θ_b represents the angle which the angular bisector of the sector (formed by the inner common tangents), makes with the x-axis. In general, the angular bisector of the sector will be distinct from the line joining the centers of A and B, and thereby have different relative velocity components. The quantities V_r, V_θ are related to $\hat{V}_r$, $\hat{V}_\theta$ (bisector quantities) as follows:

$$\begin{bmatrix} \hat{V}_r \\ \hat{V}_\theta \end{bmatrix} = \begin{bmatrix} \cos(\theta - \theta_b) & \sin(\theta - \theta_b) \\ -\sin(\theta - \theta_b) & \cos(\theta - \theta_b) \end{bmatrix} \begin{bmatrix} V_r \\ V_\theta \end{bmatrix} \tag{8}$$

In the special case when $\theta = \theta_b$ we have $V_r = \hat{V}_r$ and $V_\theta = \hat{V}_\theta$

Substituting (8) in (1), we transform the collision cone function y, so that it is now written in terms of the kinematic states as follows:

$$y = \frac{\begin{array}{c} V_\theta^2 \cos^2(\theta-\theta_b) + V_r^2 \sin^2(\theta-\theta_b) \\ + 2V_rV_\theta \cos(\theta-\theta_b)\sin(\theta-\theta_b) \end{array}}{V_r^2+V_\theta^2} - \sin^2\left(\frac{\psi}{2}\right) \quad (9)$$

A. Acceleration Laws for Collision Avoidance:

When $y<0, \hat{V}_r<0$, then this means that A is on a collision course with B. It needs to apply a suitable lateral acceleration a_{lat} to drive y to a reference value $w \geq 0$, and this will be equivalent to steering its velocity vector out of the collision cone. We employ dynamic inversion to drive y to the desired reference value of w. Differentiating (9), we obtain the dynamic evolution of y as follows:

$$\dot{y} = \frac{\partial y}{\partial \theta_b}\dot{\theta}_b + \frac{\partial y}{\partial \theta}\dot{\theta} + \frac{\partial y}{\partial V_\theta}\dot{V}_\theta + \frac{\partial y}{\partial V_r}\dot{V}_r + \frac{\partial y}{\partial \psi}\dot{\psi} \quad (10)$$

To calculate the required control input, we define an error quantity $e(t) = w - y(t)$. Taking w as a constant $\forall t$, we seek to determine a_{lat} which will ensure the error term follows the dynamics $\dot{e} = -Ke$ where $K>0$ is a constant. This in turn causes the quantity y to follow the dynamics $\dot{y} = -K(y-w)$. Note that all the partial derivatives of y can be computed analytically. While the state kinematic equations are given in (7), we however do not have analytical expressions of $\dot{\theta}_b$ and $\dot{\psi}$ and these would have to be synthesized numerically. Substituting partial derivatives, state derivatives and $\dot{y}$ in (10), we eventually get the expression for $a_{lat,A}$ as:

$$\begin{aligned} a_{lat,A} &= -(V_r^2+V_\theta^2)\frac{N_1+N_2}{D_1D_2}, \text{where} \\ N_1 &= (V_r^2+V_\theta^2)(2k(w-y)+\dot{\psi}\sin(\psi)) \\ N_2 &= \dot{\theta}_b\left(4V_\theta V_r\cos(2(\theta-\theta_b)) + 2(V_r^2-V_\theta^2)\sin(2(\theta-\theta_b))\right) \\ D_1 &= 2V_rV_\theta\cos(2(\theta-\theta_b)) + (V_r^2-V_\theta^2)\sin(2(\theta-\theta_b)) \\ D_2 &= 2\left(V_r\cos(\alpha-\theta)+V_\theta\sin(\alpha-\theta)\right) \end{aligned} \quad (11)$$

The above equation can be used for collision avoidance between A and B, wherein A takes the onus of performing the collision avoidance maneuver.

B. Acceleration laws for Rendezvous

We now consider a problem where A and B need to perform a rendezvous. We consider two versions of the rendezvous problem. In the first, rendezvous is achieved when A and B graze each other with non-zero relative velocity while in the second, rendezvous is achieved when A and B graze each other with zero relative velocity. We consider the first problem to be a cooperative rendezvous problem while the second is a non-cooperative rendezvous problem. The acceleration commands for rendezvous are also obtained using dynamic inversion, invoking a process similar to that used for the collision avoidance law.

Cooperative Rendezvous without velocity matching: In this case, the state equations for $\dot{V}_\theta$ and $\dot{V}_r$ are modified from those given in (7), and an additional state β is introduced as follows:

$$\begin{aligned} \dot{V}_\theta &= -V_\theta V_r/r - \cos(\alpha-\theta)a_{lat,A} + \cos(\beta-\theta)a_{lat,B} \\ \dot{V}_r &= V_\theta^2/r + \sin(\alpha-\theta)a_{lat,A} - \sin(\beta-\theta)a_{lat,B} \\ \dot{\beta} &= a_{lat,B}/V_B \end{aligned} \quad (12)$$

Substituting $\dot{V}_\theta$ and $\dot{V}_r$ from the above in (10), we obtain a cooperative rendezvous law as follows:

$$\begin{aligned} & a_{lat,A}\ A_{11} + a_{lat,B}\ A_{12} = -\frac{B_{11}+B_{12}(V_r^2+V_\theta^2)}{C_{11}}, \text{where} \\ & A_{11} = (V_r\cos(\alpha-\theta)+V_\theta\sin(\alpha-\theta)) \\ & A_{12} = -(V_r\cos(\beta-\theta)-V_\theta\sin(\beta-\theta)) \\ & B_{11} = \left(V_\theta^2+V_r^2\right)^2(K(w-y)+0.5\dot{\psi}\sin(\psi)) \\ & B_{12} = \dot{\theta}_b\left(\left(V_r^2-V_\theta^2\right)\sin(2(\theta-\theta_b)) + 2V_\theta V_r\cos(2(\theta-\theta_b))\right) \\ & C_{11} = \left(V_r^2-V_\theta^2\right)\sin(2(\theta-\theta_b)) + 2V_\theta V_r\cos(2(\theta-\theta_b)) \end{aligned} \quad (13)$$

In the above equation, a combination of $a_{lat,A}$ and $a_{lat,B}$ are employed to steer the relative velocity vector to the boundary of the rendezvous cone. Note that the above represents a single equation with two unknowns, meaning that there are multiple $(a_{lat,A}, a_{lat,B})$ combinations to achieve the rendezvous objective.

Non cooperative rendezvous with velocity matching: In the second version of the rendezvous problem, rendezvous is achieved when A and B graze each other with zero relative velocity. We consider the case when this is non cooperative and the onus is on A to achieve the rendezvous with B. In this case, A is assumed to have two control inputs $a_{lat,A}$ and $a_{long,A}$ which correspond to its lateral and longitudinal accelerations, respectively. In this case, the state equations for $\dot{V}_\theta$ and $\dot{V}_r$ are modified from those given in (7), and an additional state V_A is introduced as follows:

$$\begin{aligned} \dot{V}_\theta &= -V_\theta V_r/r - \cos(\alpha-\theta)a_{lat,A} - \sin(\alpha-\theta)a_{long,A} \\ \dot{V}_r &= V_\theta^2/r + \sin(\alpha-\theta)a_{lat,A} - \cos(\alpha-\theta)a_{long,A} \\ \dot{V}_A &= a_{long,A} \end{aligned} \quad (14)$$

To synthesize acceleration laws for this case, we introduce a second output function $y_2 = V_r^2+V_\theta^2$ and note that driving y_2 to zero is equivalent to A and B having zero relative velocity. We then employ dynamic inversion to determine $a_{lat,A}$ and $a_{long,A}$ so as to drive both y_1 and y_2 to zero. The eventual acceleration commands are as follows:

$$a_{lat,A}\ A_{13} + a_{long,A}\ A_{14} = -\frac{B_{13}+B_{14}(V_r^2+V_\theta^2)}{C_{12}} \quad (15)$$

$$a_{lat,A}\ A_{15} + a_{long,A}\ A_{16} = -K_2\left(V_\theta^2+V_r^2\right) \quad (16)$$

where,

$$\begin{aligned} & A_{13} = (V_r\cos(\alpha-\theta)+V_\theta\sin(\alpha-\theta)) \\ & A_{14} = (V_r\sin(\alpha-\theta)-V_\theta\cos(\alpha-\theta)) \\ & B_{13} = \left(V_\theta^2+V_r^2\right)^2(K(w-y)+0.5\dot{\psi}\sin(\psi)) \\ & B_{14} = \dot{\theta}_b\left(\left(V_r^2-V_\theta^2\right)\sin(2(\theta-\theta_b)) + 2V_\theta V_r\cos(2(\theta-\theta_b))\right) \\ & C_{12} = \left(V_r^2-V_\theta^2\right)\sin(2(\theta-\theta_b)) + 2V_\theta V_r\cos(2(\theta-\theta_b)) \end{aligned}$$

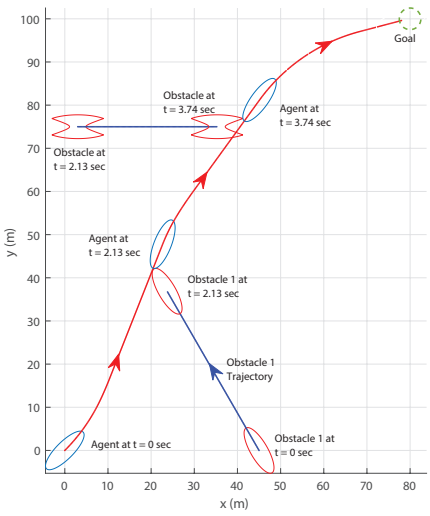

Fig. 6. Simulation 1: Trajectory

$$A_{15} = (2V_r \sin(\alpha-\theta) - 2V_\theta \cos(\alpha-\theta))$$
$$A_{16} = (2V_\theta \cos(\beta-\theta) - 2V_r \sin(\beta-\theta))$$

Eqns (15)-(16) are to be solved simultaneously to determine $a_{lat,A}(t)$ and $a_{long,A}(t)$ in order to achieve rendezvous with velocity matching.

V. Simulations

A. Simulation 1

In the first simulation, the agent F_1 is initially at $(0,0)$, with semi-major and semi-minor axes of 6 m and 2 m respectively. The speed of the agent is 25 m/s and initial heading angle is 45°. The first obstacle is an ellipse F_2 centered at $(45,0)$, moving with speed 20 m/s and heading angle 120°. The initial conditions are such that they are on a collision course which is indicated by $y(0) = -0.0452$ (negative value). Using the acceleration law (11), F_1 applies a positive lateral acceleration which initially gets saturated to a value of $15m/s^2$, and after continued acceleration, the agent comes out of the collision cone at 0.80 sec ($y > 0$), and then moves at a constant velocity until $t = 2.12$ sec. At $t = 2.13$ sec F_1 spots another obstacle F_3 (confocal quadric) at $(5,75)$ moving with a heading angle of 0° which is on collision course with F_1, indicated by $y(2.13) = -0.06$ (negative value), ψ at that instant is 36.91°. The parameters a_c, b_c, k of F_3 are 6 m, 2 m, 0.9 respectively. F_1 again computes its acceleration using (11) and comes out of the collision cone at $t = 2.70$ sec, by application of negative lateral acceleration. F_1 passes F_3 at $t = 3.74sec$ and applies maximum acceleration until it is aligned with the goal point which happens at $t = 4.88$ sec. The trajectories of F_1, F_2, F_3 are shown in Fig 6, time histories of heading angle and acceleration are in Fig 7, time history of the angle ψ is in Fig 8, time histories of y, V_r and V_θ are in Fig 9.

B. Simulation 2: Shape Changing Obstacle

In the second simulation, the shape and initial conditions of F_1 are same as in the previous simulation, while F_2 is

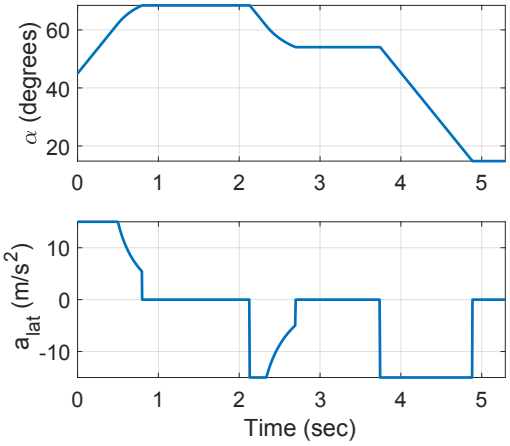

Fig. 7. Simulation 1: Commanded Acceleration and Heading angle

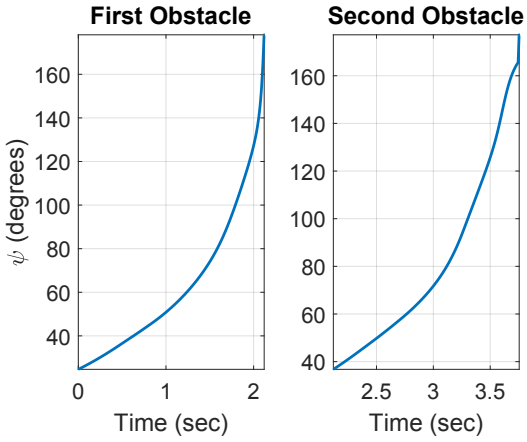

Fig. 8. Simulation 1: Time history of angle ψ

now a shape-changing confocal quadric. The shape change is governed by varying k (See 5), as $k(t) = |\sin(2t + \pi/2)|$, which causes the shape of F_2 to change from a degenerate confocal quadric to a full ellipse. The parameters a_c and b_c in (5) are 6 m and 2 m, respectively. At $t = 0$ sec, we have $k = 1$, initial speed and heading angle of F_2 are 20 m/s and 120°, respectively. The initial conditions are such that F_1 and F_2 are on a collision course which is indicated by $y(0) = -0.053$ (negative value). F_1 applies acceleration as per (11) and comes out of collision cone at 0.84 sec. The complete trajectory of F_1 and F_2 is shown in Fig 11, time histories of heading angle, acceleration and the angle ψ in Fig 12.A few snapshots showing the relative engagement of F_1 and F_2 at various time instants are shown in Fig 10.

VI. Conclusions

In this paper, we present an approach that can compute the (dynamically changing) angle between the inner common tangents to objects which are modeled as quadric surfaces (which are not necessarily the same shape). Computation of this angle is a critical component in the subsequent computation of the collision cone between the quadric surfaces. The presented approach is computationally inexpensive, which makes it usable in real-time. We subsequently develop acceleration laws that enable collision avoidance or rendezvous

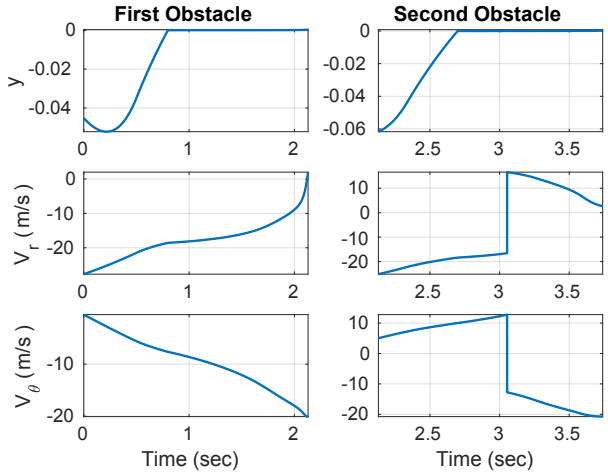

Fig. 9. Simulation 1: Collision Cone Parameters

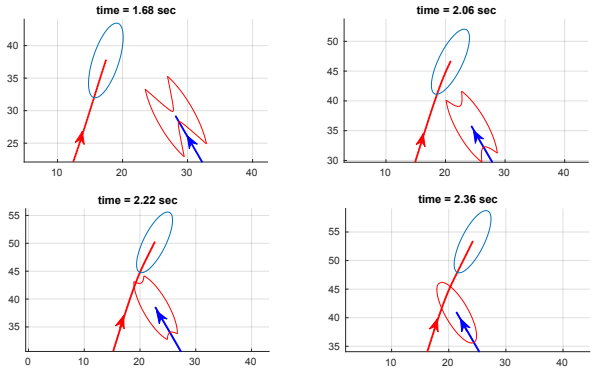

Fig. 10. Simulation 2: Snapshots of trajectory at different times

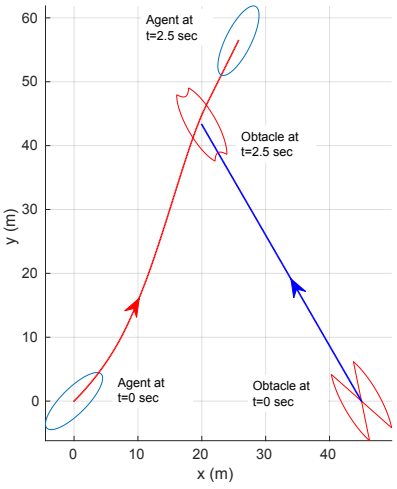

Fig. 11. Simulation 2: Trajectory

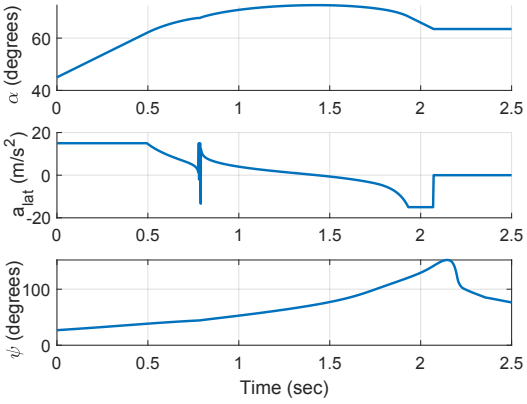

Fig. 12. Simulation 2: Commanded Acceleration, Heading angle and ψ

of quadric surfaces. Simulations are presented to demonstrate the efficacy of the guidance laws.

REFERENCES

[1] C. Goerzen, Z. Kong, and B. Mettler, "A survey of motion planning algorithms from the perspective of autonomous uav guidance," *Journal of Intelligent and Robotic Systems*, vol. 57, no. 1, pp. 65–100, 2010.

[2] M.-Y. Ju, J.-S. Liu, S.-P. Shiang, Y.-R. Chien, K.-S. Hwang, and W.-C. Lee, "A novel collision detection method based on enclosed ellipsoid," in *Proceedings of 2001 IEEE International Conference on Robotics and Automation*, vol. 3, pp. 2897–2902.

[3] Y.-K. Choi, J.-W. Chang, W. Wang, M.-S. Kim, and G. Elber, "Continuous collision detection for ellipsoids," *IEEE Transactions on visualization and Computer Graphics*, vol. 15, no. 2, 2008.

[4] H. Kumar, S. Paternain, and A. Ribeiro, "Navigation of a quadratic potential with ellipsoidal obstacles," in *2019 IEEE 58th Conference on Decision and Control (CDC)*, 2019.

[5] ——, "Navigation of a quadratic potential with star obstacles," in *2020 American Control Conference (ACC)*, 2020.

[6] A. Chakravarthy and D. Ghose, "Obstacle avoidance in a dynamic environment: A collision cone approach," *IEEE Transactions on Systems, Man, and Cybernetics-Part A: Systems and Humans*, vol. 28, no. 5, pp. 562–574, 1998.

[7] P. Fiorini and Z. Shiller, "Motion planning in dynamic environments using velocity obstacles," *The International Journal of Robotics Research*, vol. 17, no. 7, pp. 760–772, 1998.

[8] J. Van Den Berg, D. Wilkie, S. J. Guy, M. Niethammer, and D. Manocha, "Lqg-obstacles: Feedback control with collision avoidance for mobile robots with motion and sensing uncertainty," in *2012 IEEE International Conference on Robotics and Automation*. IEEE, 2012, pp. 346–353.

[9] A. Chakravarthy and D. Ghose, "Collision cones for quadric surfaces," *IEEE Transactions on Robotics*, vol. 27, no. 6, pp. 1159–1166, 2011.

[10] ——, "Generalization of the collision cone approach for motion safety in 3-d environments," *Autonomous Robots*, vol. 32, no. 3, 2012.

[11] A. Ferrara and C. Vecchio, "Second order sliding mode control of vehicles with distributed collision avoidance capabilities," *Mechatronics*, vol. 19, no. 4, pp. 471–477, 2009.

[12] Y. Watanabe, A. Calise, E. Johnson, and J. Evers, "Minimum-effort guidance for vision-based collision avoidance," in *AIAA atmospheric flight mechanics conference and exhibit*, 2006, p. 6641.

[13] P. Karmokar, K. Dhal, W. J. Beksi, and A. Chakravarthy, "Vision-based guidance for tracking dynamic objects," in *2021 International Conference on Unmanned Aircraft Systems (ICUAS)*, 2021.

[14] E. Lalish and K. A. Morgansen, "Distributed reactive collision avoidance," *Autonomous Robots*, vol. 32, no. 3, pp. 207–226, 2012.

[15] B. L. Boardman, T. L. Hedrick, D. H. Theriault, N. W. Fuller, M. Betke, and K. A. Morgansen, "Collision avoidance in biological systems using collision cones," in *2013 American Control Conference*. IEEE, 2013, pp. 2964–2971.

[16] W. Zuo, K. Dhal, A. Keow, A. Chakravarthy, and Z. Chen, "Model-based control of a robotic fish to enable 3d maneuvering through a moving orifice," *IEEE Robotics and Automation Letters*, vol. 5, no. 3, pp. 4719–4726, 2020.

[17] K. Tholen, V. Sunkara, A. Chakravarthy, and D. Ghose, "Achieving overlap of multiple, arbitrarily shaped footprints using rendezvous cones," *Journal of Guidance, Control, and Dynamics*, vol. 41, no. 6, pp. 1290–1307, 2018.

[18] J. Richter-Gebert, "Conics and their duals," in *Perspectives on Projective Geometry*. Springer, 2011, pp. 145–166.